Chapter IV

LIQUID CRYSTAL BASED TEMPERATURE AND TRANSIENT HEAT TRANSFER MEASUREMENTS ON HIGHLY CURVED SURFACES

TEST CASE : CURVED BOTTOM SURFACE OF A SQUARE TO RECTANGULAR TRANSITION DUCT

Cengiz Camci

THE PENNSYLVANIA STATE UNIVERSITY
Department of Aerospace Engineering

Summary

Accurate determination of convective heat transfer coefficients on complex curved surfaces is essential in the aero-thermal design and analysis of propulsion system components. The heat transfer surfaces are geometrically very complex in most of the propulsion applications. This study focuses on the evaluation of a hue capturing technique for the heat transfer interpretation of liquid crystal images from a complex curved heat transfer

surface. Impulsively starting heat transfer experiments in a square to rectangular transition duct are reported. The present technique is different from existing steady state hue capturing studies. A real time hue conversion process on a complex curved surface is adopted for a transient heat transfer technique with high spatial resolution. The study also focuses on the use of encapsulated, narrow color band liquid crystals in contrary to previous steady state hue based techniques using wide band liquid crystals. Using a narrow band crystal improves the accuracy of the heat transfer technique. Estimated uncertainty for the heat transfer coefficient from the technique is about 5.9 %. A complete heat transfer mapping on the bottom surface was possible by using only seven liquid crystal image frames out of the 97 available frames during the transient experiment. Significant variations of heat transfer coefficients are quantitatively visualized on the curved surfaces of the transition duct.

List of Symbols

c	specific heat
h	convective heat transfer coefficient, $h=q/(T_{o\infty}-T_w)$
HSI	hue, saturation, intensity, (normalized)
k	thermal conductivity
L	one side of the square inlet section
Nu	Nusselt number
p	local pressure
q	heat flux
R	total error in uncertainty analysis
RGB	red, green, blue, (normalized)
Re	local Reynolds number
t	time
T	temperature
TU	turbulence intensity
x,y,z	spatial coordinates
y	distance normal to the curved wall

Greek symbols

α	thermal diffusivity of air, $\alpha=k/(\rho c_p)$
β	non-dimensional time, $\beta=h(t/\rho c_p k)^{1/2}$
θ	non-dimensional wall temperature, $\theta=(T_w-T_i)/(T_{o\infty}-T_i)$
ρ	density
λ	dominant wavelength of a color

Subscripts

i	initial
o	total condition
p	at constant pressure
rec	recovery
w	local wall condition

λ spectral local value
∞ free stream

IV . 1 Introduction

This study deals with the implementation of a recently developed transient hue capturing technique on complex curved surfaces. The specific emphasis is given to apply the technique on a liquid crystal sprayed curved surface to obtain two dimensional heat transfer coefficient maps with high spatial resolution. Although there is vast amount of information in the literature about line heat transfer distributions from liquid crystal measurements, there are limited number of studies dealing with surface distributions especially on complex curved surfaces. The present technique is different from existing steady state true color heat transfer approaches. A real time hue conversion process is adopted for high resolution heat transfer measurements using a transient heat transfer model.

The molecular structure, optical and thermal properties of cholesteric liquid crystals have been extensively reviewed by Fergason (1964,1968). A general discussion on the use of liquid crystals for heat transfer purposes is given in Cooper et al. (1975), Simonich and Moffat (1984), Moffat (1990), Hippensteele et al. (1983,1985,1987) and Parsley (1991). Unencapsulated (neat) liquid crystals can be used to indicate shear stress and hence transition in wind tunnel tests and actual flight testing, Jones et al. (1992), Klein and Margozzi (1970), Holmes et al. (1986,1987). However, encapsulated forms of cholesteric and chiral nematic liquid crystals show a very useful feature from a heat transfer point of view. They are relatively insensitive to normal and shearing stresses, Zharkova et al. (1980). The color response of liquid crystals to temperature is very fast and the response time is no more than a few milliseconds, Ireland and Jones (1987).

Application of liquid crystals in transient heat transfer experiments is discussed by Ireland and Jones (1985) and Jones and Hippensteele (1987). In a transient experiment a complete heat transfer mapping of a complex surface can be obtained from a set of video images. However, in steady state mode, multiple experiments with different heat flux settings are required to completely map the surface. Each new constant heat flux setting may also generate a new wall to free stream temperature ratio. Transient experiments usually generate an approximately isothermal surface boundary condition. The deviation from an isothermal wall temperature is most of the time small when compared to the temperature difference between the wall and the free stream. Transient heat transfer techniques are also attractive from operating cost point of view, especially when a large mass flow of heated air at high speed is required. Mechanical construction of a constant heat flux surface on a highly curved three dimensional surface is considerably more difficult when compared to the simple liquid crystal spraying procedure for a typical transient experiment. Transient techniques used in the past employing discrete sensors or liquid crystal indicators never reached the spatial resolution (512x480 sensors per image) of the current method. The high spatial resolution of the present transient method having pixel by pixel processing capability is also applicable in unsteady heat transfer research for temperature fluctuation levels having a typical frequency of less than 60 Hz.

In most of the previous studies reviewed, a visual detection of yellow contour was the most quantitative description of a narrow isothermal band that could be captured from a specific image. Wang et al. (1990) used a technique to mark the pixels for the appearance of a light intensity peak. Bunker et al. (1990) introduced another single color capturing technique using a chrominance-luminance technique developed by Hirsch (1987).

Calibrating the hue from colors appearing on a liquid crystal sprayed surface with respective to temperature has been frequently practiced in the past. The wavelength of the color from a liquid crystal covered surface was correlated with local temperature by Kuzniers et al. (1980). This study employed local temperature measurements in the field of plastic and restorative surgery. Buiko et al. (1980) used cholesteric liquid crystals for temperature mapping in the diagnosis of neoplasms of the human eye. The temperature dependency of the dominant wavelength of the light selectively reflected from the surface was obtained by a spectrophotometer. Hollingsworth, Boehman, Smith and Moffat (1989) used a hue versus temperature relation in a steady state convective heat transfer experiment for the first time. They could calculate the hue angle of a liquid crystal color starting from RGB attributes provided by standard video equipment. Their technique was useful for steady state heat transfer measurements taken at a limited number of points on a heat transfer surface.

Most of the spectrum of colors appearing on a liquid crystal sprayed surface can be used to obtain many isotherms simultaneously. A hue capturing technique based on the real time determination of the dominant wavelength of each color appearing on a liquid crystal surface is described by Camci et al. (1991). An extensive experimental validation of this heat transfer mapping technique is presented in Kim (1991), for a well documented test case of a round circular heated jet impinging on a flat plate, initially kept at ambient temperature. Liquid crystal based heat transfer distributions are compared with results from conventional surface mounted thermocouple based distributions. Additional comparisons are also made to other studies available in the literature. A detailed uncertainty analysis for the heat transfer technique is also presented. A complete numerical heat transfer simulation of the impinging jet heat transfer experiment is also provided by Kim (1991). Simulations include a differential solution for the transient energy equation in addition to momentum and continuity equations. As a result of a set of validation experiments and computations, it has been shown that the hue capturing method is an accurate and powerful tool in obtaining line distributions of heat transfer with high spatial resolution.

The current study deals with the implementation of the hue capturing technique developed by Camci et al. (1991) on a complex curved surface. The bottom surface of a square to rectangular transition duct is used for two dimensional surface mapping of heat transfer coefficients. The current study combines a real time hue conversion process with a transient heat transfer model developed for complex curved surfaces. The study also focuses on the use of narrow band encapsulated liquid crystals for better accuracy in hue versus temperature calibration. The standard deviation of hue around a mean hue versus temperature line is about 1/10 th of the bandwidth of the liquid crystal as reported by Camci et al. (1991), for an encapsulated chiral nematic liquid crystal.

IV . 2 Wind Tunnel and Transition Duct

A continuous flow wind tunnel is adapted such that flow can be switched suddenly through the test section. The wind tunnel and transition duct connected to a main laboratory vacuum system are shown in Figure 4.1. Ambient temperature air is drawn from the laboratory through the test section. The transient experiment is started by opening a pneumatically controlled fast acting valve at three meters downstream of the test section.

The model tested was a transition duct from a (20.8 cm x 20.8 cm) square to a rectangular cross section of (32.2 cm x 10.7 cm). The heat transfer at the bottom wall of the transition duct was

measured. The details of the duct geometry are given in Figure 4.2. A microswitch on the valve sent a simultaneous trigger pulse for the start of the data acquisition sequence. A precision timer was also started at this specific time to time stamp the video frames. The chiral nematic liquid crystal images were recorded by a color video camera located in an approximately normal direction to the transition duct floor and transmitted to a high resolution video recorder. Model illumination was provided by fluorescence lights located about 50 cm away from the duct floor.

The transition duct was preheated by using an electronically controlled electric heater chamber in the form of two half cylinders. Blanket heaters as radiation heaters provided a sufficiently uniform model temperature after a five-hour initial heating period. The temperature uniformity was continuously monitored at 10 discrete locations on the model surface. A standard initial temperature deviation of only + 0.2 ^{o} C was allowed. The transition duct model was precision machined from clear acrylic. A thermophysical triple product $(\rho c_p k)^{1/2}$ value of 569 $W(sec)^{1/2}/(m^2K)$ was used in data reduction as reported by Baughn, Ireland, Jones and Saniei (1988). Transient conduction analysis showed that the thermal wave did not reach the back end of the test wall during the heat transfer experiment, Jones and Hippensteele (1985). A cross section of the heat transfer surface with liquid crystal coating is shown in Figure 4.2.

IV . 3 Color Definition and Hue Capturing Process

Color may be defined as a psychophysical property of light specifically, the combination of those characteristics of light that produces the sensations of hue, saturation and intensity in a normal human observer. Color sensation from a liquid crystal covered surface is generated by several characteristics. A few of these characteristics can be summarized as the pitch of the helical arrangement of the crystal structure, the spectral characteristics of the light illuminating the liquid crystal covered surface and the spectral response of the color sensing component which may be human eye or an imaging sensor used in a color camera. The pitch of the helical arrangement in the liquid crystal structure is altered by local temperature on the heat transfer surface. The color recognition technique used in this study is further explained in Camci et al. (1991), Kim (1991) and Berns (1989). The present system uses three eight bit video A/D converters. Each of the RGB attributes is scaled between 0 and 255. The real time conversions from RGB attributes to HSI and the role of intensity and saturation in liquid crystal color interpretation are discussed in Camci et al. , (1991).

IV . 4 Transient Heat Transfer Technique

The main assumption of the measurement technique is the small penetration depth of the thermal pulse into the plexiglass wall compared to the thickness of the wall. This assumption allows the use of a one-dimensional transient heat transfer theory developed for semi-infinite bodies. The local wall

temperature rise for an impulsively starting heat transfer experiment can be related to time, thermophysical properties of the body and the convective heat transfer coefficient h.

(4.1)

where θ and $\beta=h(t/\rho c_p k)^{1/2}$ are non-dimensional temperature and time respectively. A sixth order spline fitting routine was developed for the variation of non-dimensional time β with respect to the non-dimensional wall temperature θ, using equation 1. Attention was paid to obtain an accurate representation for the first 15 seconds of a typical experiment.

(4.2)

Experimental Results and Discussion

IV.5.1 ***<u>Mainstream Flow and Thermal Boundary Conditions :</u>*** A continuous recording of the tunnel inlet temperature, inlet velocity from a pitot probe and fast valve initial transient behavior were obtained. Tunnel total temperature measured upstream of the inlet section was the same as the ambient temperature ($T_{o\infty}$=28.6 ^{o} C). The inlet velocity measured at the inlet probe section by using a pitot probe was free of transients after the first second measured from the valve opening time as shown in Figure 4.3. However, additional inlet velocity measurements taken by a fast response hot wire showed that the actual start-up transients are confined to a 40 millisecond period after the valve opening.

The mean velocity component parallel to the tunnel axis measured at the freestream of the inlet probe section was about 97.5 m/sec. Figure 4. 4 shows a mean velocity traverse taken along the height of the duct centerline. The inlet boundary layer thickness at the bottom wall of the inlet probe section was measured to be 8.9 mm. It was also confirmed that the top wall boundary layer has a very similar distribution. The measured free stream turbulence intensity in the mainstream of the inlet probe section was about 1.0 %. The initial temperature for the liquid crystal covered bottom surface of the duct was about T_i=55.7 ^{o} C.

Three dimensional mean flow in the duct was predicted by solving Navier-Stokes equations in a staggered grid (49x26x26), Kim (1991). Due to the symmetry of the duct, only one quadrant of the field was predicted in a generalized coordinate system as presented in Figure 4.5. A kinetic energy-dissipation rate model was used for turbulent flow modelling. Turbulent kinetic energy at the inflow boundary was computed from measured root mean square values of the velocity fluctuation based on the isotropic field assumption. The inlet centerline velocity of

97.5 m/sec is accelerated to 123 m/sec at the exit section due to the overall area convergence of 0.716, Figure 4.5.a. Two counter rotating vortices in the exit quadrant were identified. However the absolute magnitude of the maximum secondary velocity (3.6 m/sec) was found to be much smaller than that of the streamwise velocity, Figure 4.5.c.

IV.5.2 Liquid Crystal Calibration : Hue versus temperature calibrations were performed to find out the dependency of local liquid crystal hue to temperature. A mixture of three chiral nematic liquid crystals each having a color bandwidth of approximately 1 ^{o} C was then sprayed simultaneously. Estimated thickness of the liquid crystal layer was in the order of 10 microns. The highest temperature crystal displayed red color at 47.8 ^{o} C. The medium temperature and the lowest temperature crystal displayed red at 42.7 ^{o} C and 37.5 ^{o} C, respectively. The imaging camera was located on top of the duct in a direction almost normal to the bottom surface. The exact same illumination system of actual heat transfer runs was used. A heat gun with an approximate exit temperature of 85 ^{o} C was directed to a T type thin foil thermocouple with a typical time response of 1 millisecond. The thermocouple was flush mounted underneath the liquid crystal layer, at this specific pixel location. Figure 4.6.a shows the variation of local temperature measured by the thermocouple with respect to liquid crystal hue as recorded by the hue capturing system. Different symbols in Figure 4.6 suggest different hue capturing sequences performed at different times. The color information as hue shows an approximately linear variation with respect to local temperature between 37.7 ^{o} C and 38.3 ^{o} C. It is a known phenomenon that the perceived color especially from an unencapsulated (neat) liquid crystal is dependent on the angle at which it is viewed, Jones et al. (1992), Herald and Wiegel (1980). However, our visual observations consistently showed that the viewing angle sensitivity of hue from micro encapsulated chiral nematic liquid crystals is much less significant than that of the unencapsulated (neat) crystals.

Figure 4.6.b shows the variation of local intensity with respect to local temperature for all three of the liquid crystals. A very distinct intensity peak for each liquid crystal range was always observed. After the peak, the intensities dropped continuously to a middle value between the lowest intensity and the peak intensity value. This final value corresponded to the dark blue color. For the highest temperature crystal, total number of hue values captured were limited in comparison to the wide spectrum of colors obtained with the middle and lowest temperature crystals. Faded colors were attributed to the highest level of temperature gradient applied along a direction normal to the liquid crystal coated surface. However, the hue values between 130 and 160 provided a successful temperature calibration for the highest temperature liquid crystal.

IV.5.3 High Resolution Heat Transfer Maps at the Bottom Surface of the Transition Duct : The experiment with an initially heated test section, T_i=55.7 ^{o} C, was started by suddenly connecting the test section to a large vacuum reservoir providing continuous steady flow at $T_{o\infty}$=28.6 ^{o} C. The heat flow direction was from the wall to the free stream. The highest temperature liquid crystal responded between t=3.38 and t=6.25 seconds as shown in Figure 4.7.

The figure presents only eight of the 97 available video images and the associated quantitative heat transfer islands. The centerline of the duct is shown with a solid line in the figure.

Since hue determination at low intensity values is not a stable process, Berns (1989), any hue value having an associated intensity value of 50 or less was discarded during the data reduction. Each pixel staying within the hue range between 140 and 150 was marked and its pixel coordinate was written into a computer file. 10 units wide hue range corresponded to an approximate temperature interval of 0.31 ^{o} C for the highest temperature crystal. The pixels marked with the criteria described above were also presented on the left-hand side of each color image. Temperature of each individual pixel was deduced from the calibration information shown in Figure 4.6.a. The convective heat transfer coefficient was obtained by using the transient technique described in a previous section.

When the fast valve opened, the image from the bottom surface was completely dominated by black. The appearance of the first dark blue color was within the first second. The dark blue color was dominant almost uniformly all over the bottom surface. Blue content of the liquid crystal color did not change for a long period between t=0.0 and t=3.30 seconds due to a negligible hue-temperature slope around 49 ^{o} C. The colors in this band could approximately be described by greenish-blue as shown for the image taken at t=3.38 seconds in Figure 4.7. This specific color band corresponded to the local temperatures between 48.25 and 48.56 ^{o} C. The calculated heat transfer coefficient limits for the specific hue range, at t=3.38 sec. were between 99 and 94 W/m^{2}K. The specific heat transfer coefficient island shown at t=3.38 sec. corresponded to the coldest zone of the duct bottom surface. This island generated the highest heat transfer coefficient. As the time passed, the cold front (48.25 - 48.56 ^{o} C) diffused more into the inlet section of the duct. At t=3.43 and t=3.56 seconds the spread of the cold front was not very distinct due to small time steps in the order of 50 and 130 milliseconds. At t=3.66 seconds, the cold front was not any more in the shape of a single closed island. The cold front was more diffused in a form which complemented the island representing the previous heat transfer distribution for t=3.38 sec. Besides this island marked as (X), a narrow band of the same cold front (Y) was apparent close to the upper right corner of the image. The images for t=3.66, 3.88 and 4.22 seconds show the temporal growth of the islands marked as (X) and (Y). During this period, the region (Y) did not significantly alter its shape. However, the (X) started to grow more into the inlet section of the duct. Regions (X) and (Y) gradually merged into each other at t=4.22. Furthermore, the left-hand edge of the island (X) extended itself up to the square inlet section of the duct. The frames captured at t=4.55 and 5.32 seconds showed the movement of the island (X) further into the square inlet section. Gradual transition into smaller heat transfer coefficient islands with increasing time continued as shown in the image for t=5.32 seconds. The islands (X1) and (X2) gradually reduced their areas as time passed. At t=6.25 seconds, the island (X2) became a relatively small region near the symmetry line of the duct. The data density of useful heat transfer information from the highest temperature crystal was extremely high. Further combined presentation of data is shown in Figure 4.8. As far as the h bandwidths are concerned, the corresponding heat transfer coefficient islands were distinctly marked without any significant

overlapping. The blank areas which were not filled with symbols also automatically generated extra heat transfer coefficient islands between the marked areas.

As a general result, the highest convective heat transfer coefficients were observed near the exit section of the bottom surface. This area corresponded to a flow zone where the duct width was maximum in the horizontal plane and minimum in the vertical plane. The highest heat transfer coefficients appeared in an area where there was strong main stream acceleration on the curved bottom surface. Entrance section of the duct resulted in the lowest level of convective heat transfer activity. As it is shown in the images for t=5.32, 5.72 and 6.25 seconds, the lowest heat transfer islands were organized along the first one third of the duct length around the symmetry line, (X1 and X2). The flow and its corresponding convective heat transfer activity were symmetrical in the transition duct. The corner flow regions near the curved duct boundary shown in Figure 4.7 experienced minimal convective heat transfer coefficients.

time	island mark	time step	h range	h band	Figure
sec.		msec.	W/m^2K		
3.38	1	---	99-94	5	4.7
3.66	2	280	95-90	5	4.8
4.22	3	560	89-84	5	4.7
4.55	4	330	85-81	4	4.8
5.32	5	770	79-75	4	4.7
5.45	6	130	78-74	4	4.8
6.25	7	670	73-69	6	4.7

Table 1

Time and heat transfer information for 7 the frames shown in Figures 4.11 and 5.12.

IV . 6 Uncertainty Analysis

Typical uncertainties from the technique introduced, at better than 90 % confidence level are estimated as:

$\delta(T_{o\infty} - T_i)/(T_{o\infty} - T_i) = \pm 1.5\ \%$ $\delta(T_w - T_i)/(T_w - T_i) = \pm 1.0\ \%$

$\delta((\rho c_p k)^{1/2})/(\rho c_p k)^{1/2} = \pm 5.0\ \%$ $\delta t/t = \pm 1.5\ \%$

The uncertainty of heat transfer coefficient can be obtained from the combination of the listed errors, Kline and McClintock (1953). The uncertainty of the non-dimensional temperature $\theta = (T_w - T_i)/(T_{o\infty} T_i)$ can be calculated as ($\delta\theta/\theta = 1.80\ \%$). The uncertainty of the non-dimensional time β is based on equation 1, ($\delta\beta/\beta = (1/\beta)(\delta\beta/\delta\theta)(\delta\theta) = 2.74\ \%$). The combination rule results in the final uncertainty estimate.

$$\delta h/h = \{[(\delta(\rho c_p k)^{1/2}/(\rho c_p k)^{1/2}]^2+[\delta t/t]^2+[\delta\beta/\beta]^2\}^{1/2} = 5.89\ \%$$

IV . 7 Conclusions

A recently developed digital image processing based real time color capturing method was implemented to obtain convective heat transfer coefficients from liquid crystal coated surfaces in a transition duct with a complex geometry. The method, previously validated for simple geometries and line distributions was successfully implemented on curved surfaces.

A real time hue capturing technique was employed in a transient heat transfer experiment.

The high spatial resolution of the present transient method with pixel by pixel processing capability is also applicable in unsteady heat transfer research for wall temperature fluctuation levels having a typical frequency of less than 60 Hz.

A repeatable hue versus temperature calibration process for the crystal mixture provided an accurate heat transfer tool with an estimated uncertainty of + 5.9 % on convective heat transfer coefficient.

A complete heat transfer mapping of the bottom surface was possible with excellent spatial resolution, using only seven liquid crystal image frames out of 97 available from the passage of the highest temperature crystal colors.

An approximately three second long color passage period from a single crystal was adequate for the complete mapping effort. The reduced data as convective heat transfer coefficient islands on the surface was presented with its associated natural color image captured for each specific time. Consistency and repeatability of the method in terms of marking the pixels within a predetermined narrow temperature band were proven.

Highest convective heat transfer coefficients were induced near the exit section of the bottom surface, occupying a central region having one third of the duct length as a characteristic length. This area corresponded to a flow zone where the duct width was maximum in the horizontal plane and minimum in the vertical plane. This zone of the bottom wall was exposed to a flow with significant mainstream acceleration. The lowest level of convective heat transfer was observed near the entrance section of the duct along the first one third of the duct length around the symmetry line. There was also a second zone with relatively low convective heating activity near the upper curved boundary, (X1, t=6.25 second). The corner flow region experienced

minimal convective heat transfer coefficient levels.

References

Baughn, J.W., Ireland, P.T., Jones, T.V. and Saniei, N., 1988, "A Comparison of the Transient and Heated Coating Methods for the Measurement of Local Heat Transfer Coefficients on a Pin Fin," ASME paper 88-GT-180.

Buiko, A.S., Tsykalo, A.L., 1980, "Color Thermography of Liquid Crystals in Diagnosis of Neoplasms of Eye and Eye Socket," Advances in Liquid Crystal Research and Applications, Vol.2, Edited by: L.Bata, *Pergamon Press*, Oxford, pp.1301-1304.

Berns, R.S., 1989, "Colorimetry for Electronic Imaging Devices," Tutorial Short Course Notes (T60), Center for Imaging Science/Rochester Institute of Technology, The International Society for Optical Engineering, OE/LASE '89.

Bunker, R.S., Metzger, D.E., Wittig, S., 1990, "Local Heat Transfer in Turbine Disk-Cavities. part I : Rotor and Stator Cooling with Hub Injection of Coolant," ASME paper 90-GT-25, to be published in the transactions of the ASME.

Camci, C., Kim, K., Hippensteele, S.A., 1992, "A New Hue Capturing Technique for the Quantitative Interpretation of Liquid Crystal Images Used in Convective Heat Transfer Studies," ASME GT-122, also in the Transactions of the ASME, Journal of Turbomachinery, Vol. 114, No.4, pp.512-518.

Cooper, T.E., Field, R.J., Meyer, J.F, 1975, "Liquid Crystal Thermography and Its Application to the Study of Convective Heat Transfer, " *Trans. of the ASME, Journal of Heat Transfer,* Vol.97, pp.442-4

Fergason, J.L., 1964, "Liquid Crystals," *Scientific American*, Vol.211, No.2, pp. 76-85.

Fergason, J.L., 1968, "Liquid Crystals in Non-destructive Testing," *Applied Optics*, Vol.7, No.9, pp.1729-1737.

Herald, W., Wiegel, D., 1980, "Problems of the Photographic Documentation of Liquid Crystalline Thermographs," Advances in Liquid Crystal Research and Applications, Vol.2, Edited by: L.Bata, *Pergamon Press*, Oxford, pp.1255-1259.

Hippensteele, S.A., Russell, L.M., Stepka, F.S., 1983, "Evaluation of a Method for Heat Transfer Measurements and Thermal Visualization Using a Composite of a Heater Element and Liquid Crystals, " *Trans. of the ASME, Journal of Heat Transfer*, Vol.105, pp.184-189.

Hippensteele, S.A., Russell, L.M., Torres, F.J., 1985, "Local Heat Transfer Measurements on a Large Scale-Model Turbine Blade Airfoil Using a Composite of a Heater Element and Liquid-Crystals, " *Trans. of the ASME, Journal of Engineering for Gas Turbines and Power,* Vol.107,

pp.953-960.

Hippensteele, S.A., Russell, L.M., Torres, F.J., 1987, "Use of a Liquid-Crystal,Heater-Element Composite for Quantitative, High-Resolution Heat Transfer Coefficients on a Turbine Airfoil, Including Turbulence and Surface Roughness Effects, " *NASA Technical Memorandum* 87355 .

Hirsch, C., 1987, "Aufbau und Inbetriebnahme eines Versuchsstandes zur instätionaren Wärmeübergangsmessung an rotierenden Scheiben bei erzwungener Konvektion und Prallkühlung unter Nutzung thermochromer Flüssigkristalle als Temperaturindikatoren," Diplomarbeit No. 302, Institut für Thermische Strömungsmaschinen, Universität Karlsruhe.

Hollingsworth, D.K., Boehman, A.L., Smith, E.G., Moffat, R.J.,, 1989 "Measurement of Temperature and Heat Transfer Coefficient Distributions in a Complex Flow Using Liquid Crystal Thermography and True-Color Image Processing," Collected Papers in Heat Transfer, ASME HTD-Vol.123, pp. 35-42.

Holmes, B.J., and Gall, P.D., 1986, "Liquid Crystals for High Altitude in Flight Boundary Layer Flow Visualization," AIAA General Aviation Technology Conference, AIAA paper 86-2592.

Holmes, B.J. and Obara,C.J., 1987, "Advances in Flow Visualization Using Liquid Crystal Coating," SAE General Aviation Aircraft Meeting, Wichita, SAE paper 87-1017.

Ireland, P.T., Jones, T.V., 1985, "The Measurement of Local Heat Transfer Coefficients in Blade Cooling Geometries, " AGARD Conference Proceedings on Heat Transfer and Cooling, CP 390 Paper 28, Bergen, Norway.

Ireland, P.T. and Jones, T.V., 1987, "The Response Time of a Surface Thermometer Employing Encapsulated Thermochromic Liquid Crystals,". *J. Phys. E: Sci. Instrm*., Vol.20.

Jones, T.V., Hippensteele, S.A., 1985, "High-Resolution Heat Transfer-Coefficient Maps Applicable to Compound-Curve Surfaces Using Liquid Crystals in a Transient Wind Tunnel, " Developments in Experimental Techniques in Heat Transfer and Combustion-HTD-Vol.71, ASME book no. H00390.

Jones, T.V., Hippensteele, S.A., 1988, "High-Resolution Heat Transfer-Coefficient Maps Applicable to Compound-Curve Surfaces Using Liquid Crystals in a Transient Wind Tunnel," *Nasa Technical Memorandum* 89855.

Jones, T.V., Ireland, P.T., Wang, Z., 1992, "Liquid Crystal Techniques, " Keynote paper, Proceedings of the International Symposium on Heat Transfer in Turbomachinery, held in Athens, Greece, 24-28 August 1992.

Kim, K., 1991, "A New Hue Capturing Technique for the Quantitative Interpretation of Liquid Crystal Images Used in Convective Heat Transfer Studies," Ph.D. Thesis, The Pennsylvania State University, Aerospace Engineering Department.

Klein, E.J., and Margozzi, A.P., 1970, Review of Scientific Instruments, Vol.44, pp:238-243.

Kline, S.J., and McClintock, F.A., 1953, "Describing Uncertainties in Single Sample Experiments," *ASME, Mechanical Engineering*, Vol. 75, pp.3-8.

Kuzniers, J., Drzymala, A., Grossman, B., Lipinski, A., 1980, "The Application of Liquid-

Crystalline Temperature Indicators to Medical Diagnosis," Advances in Liquid Crystal Research and Applications, Vol.2, Edited by: L.Bata, *Pergamon Press*, Oxford, pp.1277-1281.

Moffat, R.J., 1990, "Experimental Heat Transfer," Heat Transfer 1990, Proceedings of the Ninth International Heat Transfer Conference, Keynote paper-11, Edited by: G.Hetsroni, pp.187-204.

Parsley, M., 1991, "The Use of the Thermochromic Liquid Crystals in Research Applications, Thermal Mapping and Non-destructive Testing," Seventh IEEE , SEMI-THERM Symposium, pp.53-58.

Simonich, J.C., Moffat, R.J., 1984, "Liquid Crystal Visualization of Surface Heat Transfer on a Concavely Curved Turbulent Boundary Layer, " *Trans. of the ASME, Journal of Eng. for Gas Turbines and Power*, Vol.106, pp.619-627.

Wang, Z., Ireland, P.T., Jones, T.V., 1990, "A Technique for Measuring Convective Heat-Transfer at Rough Surfaces," ASME paper 90-GT-300.

Zharkova, G.M., Khachaturyan, V.M., Vostokov, L.A., Alekseev, M.M., 1980, "Study of Liquid Thermoindicators," Advances in Liquid Crystal Research and Applications, Vol.2, Edited by: L.Bata, *Pergamon Press,* Oxford, pp.1221-1239.

Fig. 4.1 Heat transfer tunnel and the transition duct

Fig. 4.2 Details of the duct geometry and the heat transfer surface

Fig. 4.3 Free stream velocity at the inlet probe section

Fig. 4.4 Boundary layer profile at the inlet probe section

(only the bottom wall profile is shown)

Fig. 4.5 Three dimensional flow predictions in the duct
a. horizontal plane, b. vertical plane, c. secondary velocities

Fig. 4.6 Hue and intensity calibration with respect to temperature

Fig. 4.7.a Convective heat transfer coefficient distributions
t=3.38, 3.66, 3.88, 4.22 sec.

Fig. 4.7.b Convective heat transfer coefficient distributions
t=4.55, 5.32, 5.72, 6.25 sec.

Fig. 4.8 Heat Transfer map at the bottom surface of the transition duct

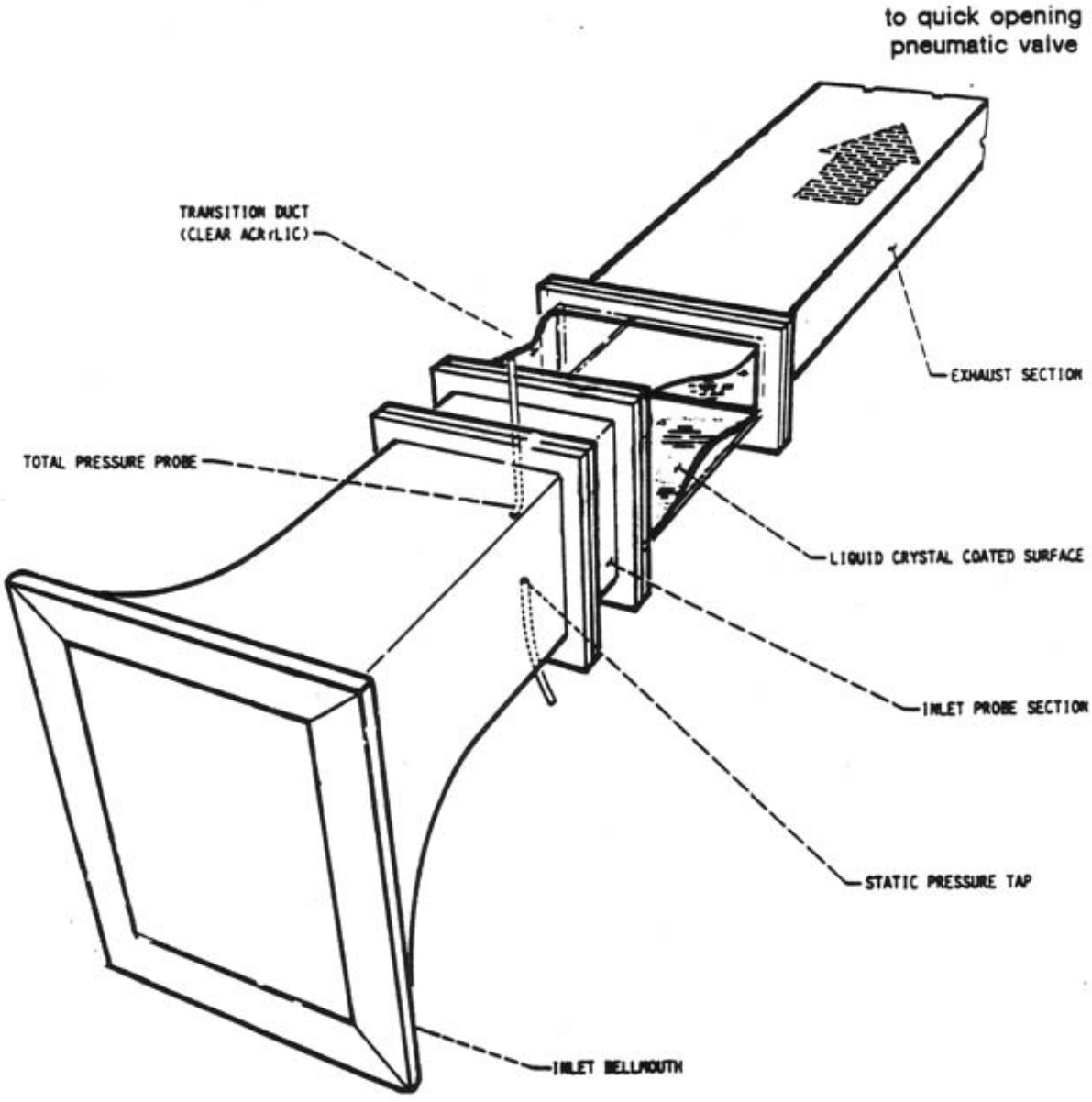

Fig. 4.1 Heat transfer tunnel and the transition duct

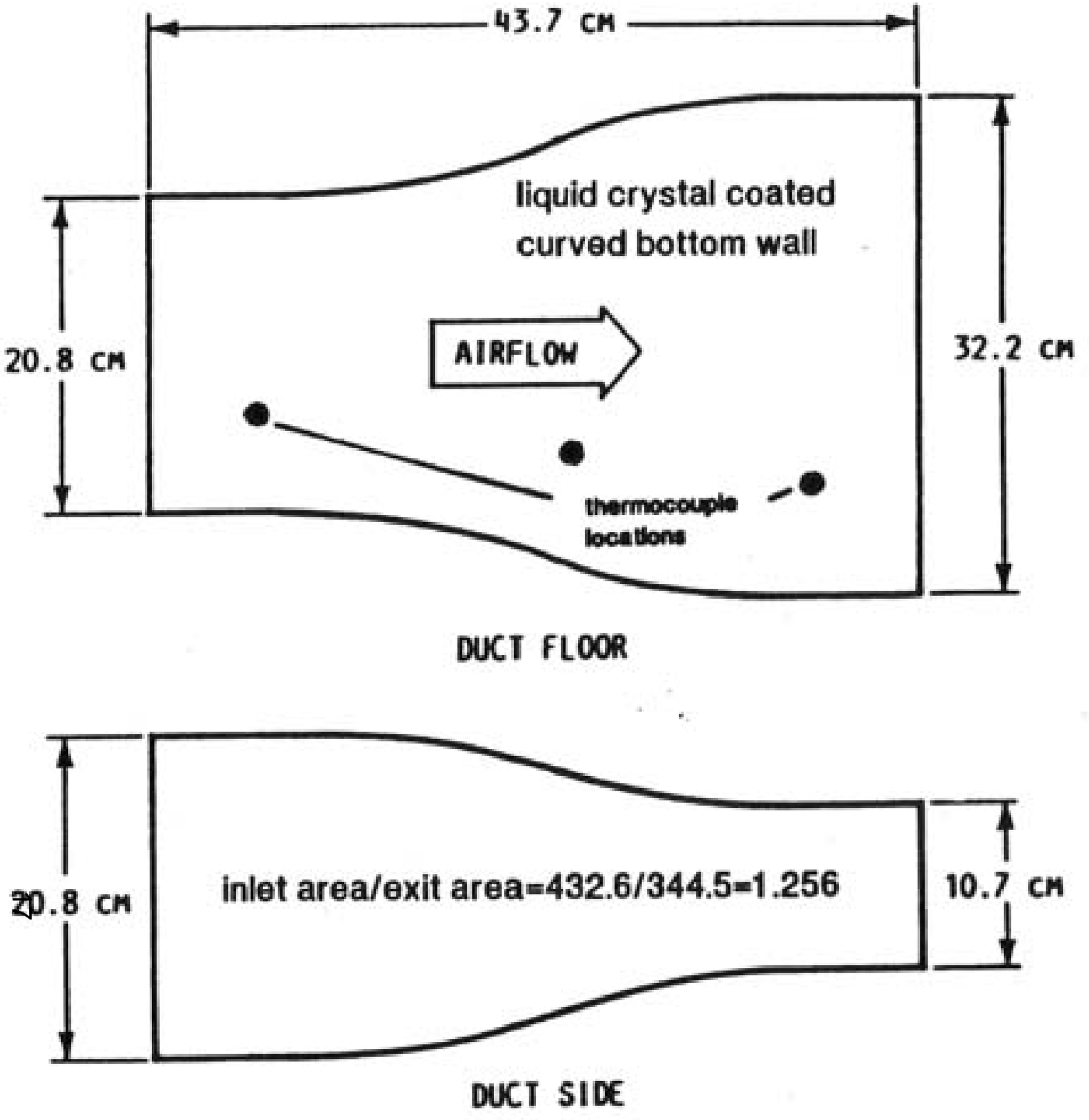
43.7 CM
liquid crystal coated
curved bottom wall
AIRFLOW
20.8 CM
32.2 CM
thermocouple
locations
DUCT FLOOR
20.8 CM
inlet area/exit area=432.6/344.5=1.256
10.7 CM
DUCT SIDE

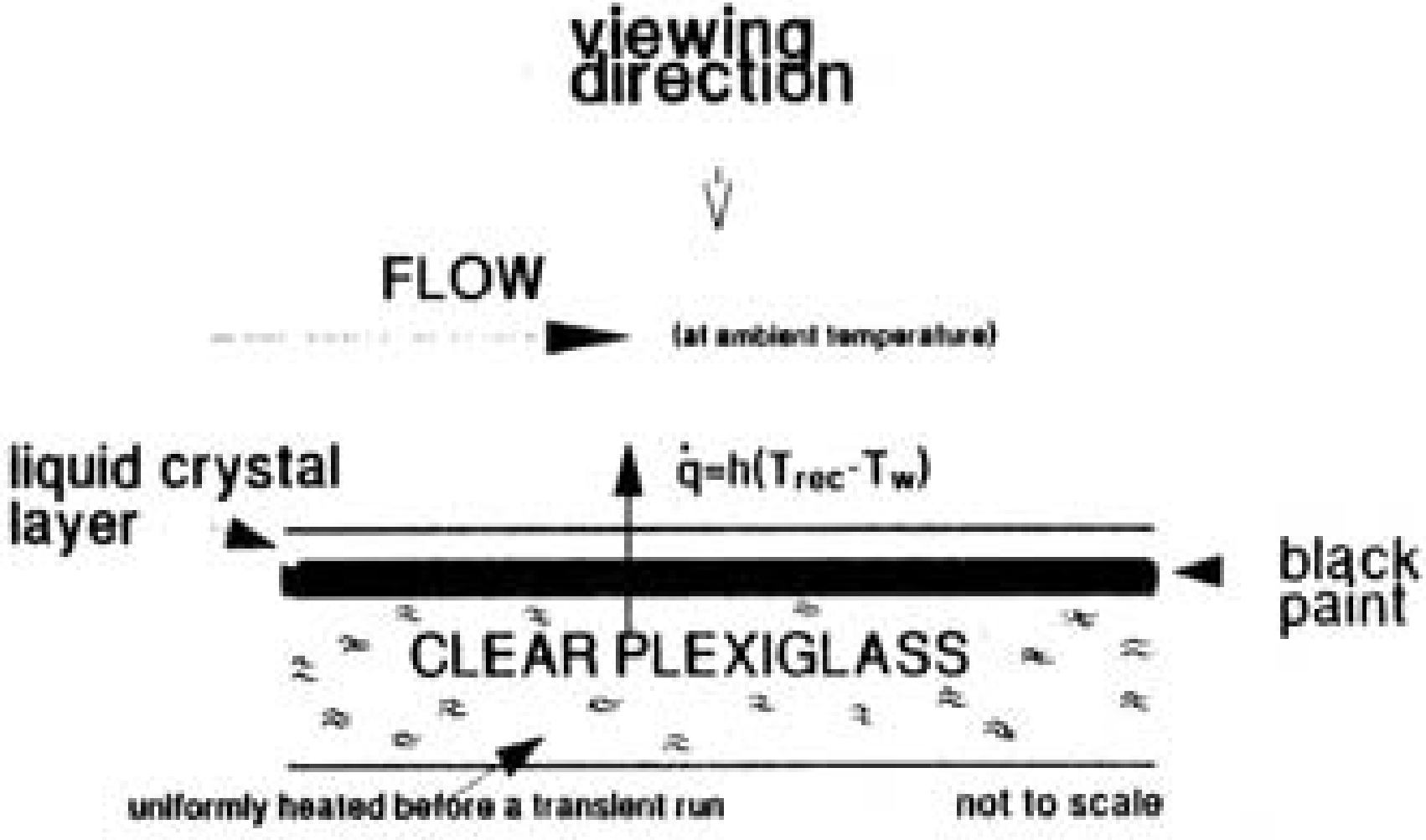
viewing direction
FLOW
(at ambient temperature)
liquid crystal layer
$\dot{q}=h(T_{rec}-T_w)$
black paint
CLEAR PLEXIGLASS
uniformly heated before a transient run
not to scale
HEAT TRANSFER SURFACE

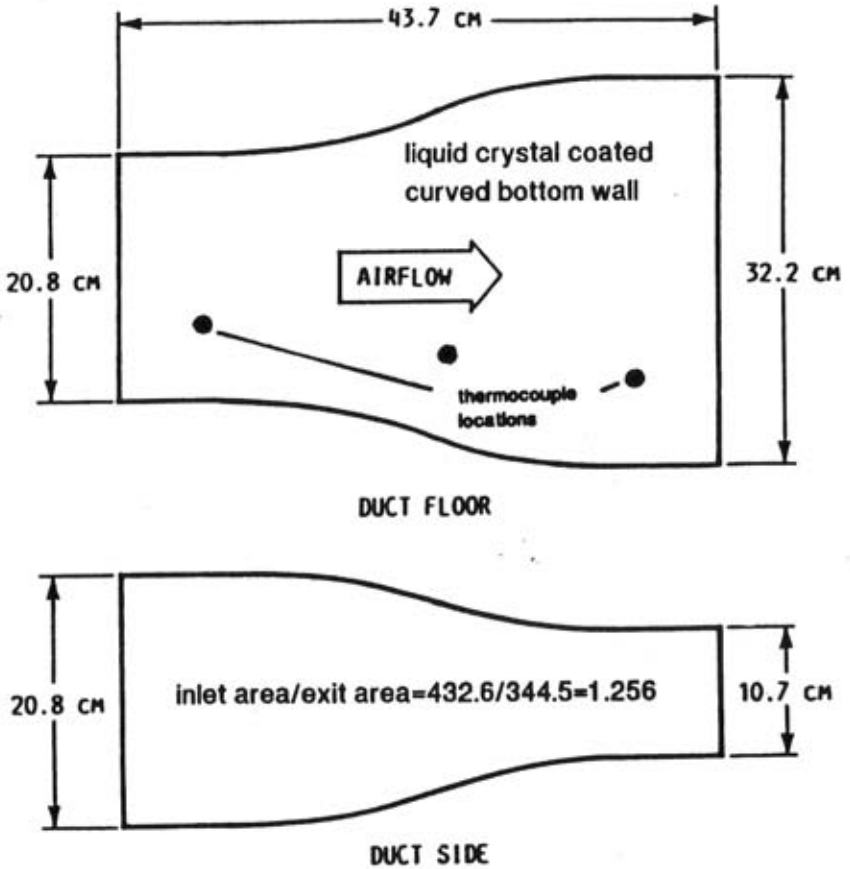

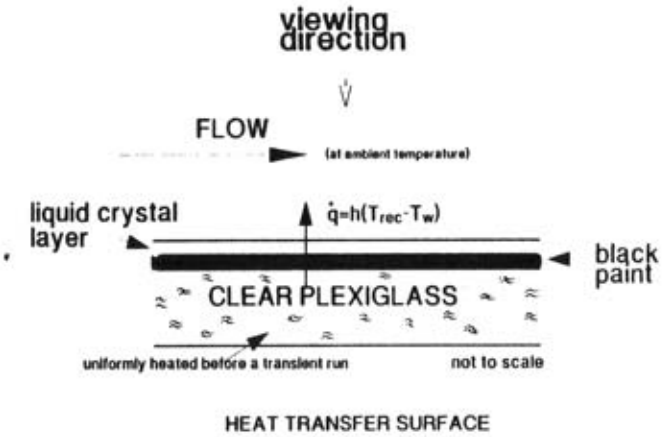

Fig. 4.2 Details of the duct geometry and the heat transfer surface

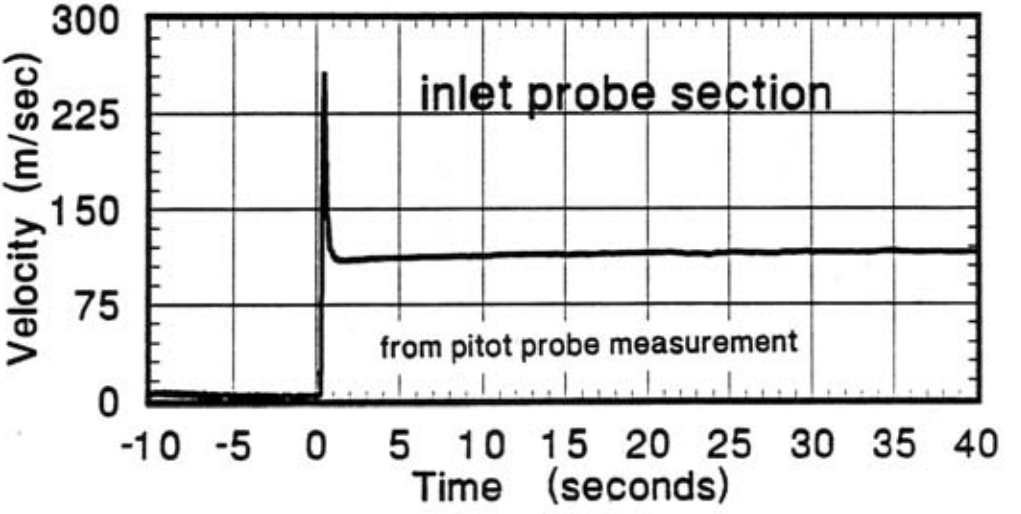

Fig. 4.3 Free stream velocity at the inlet probe section

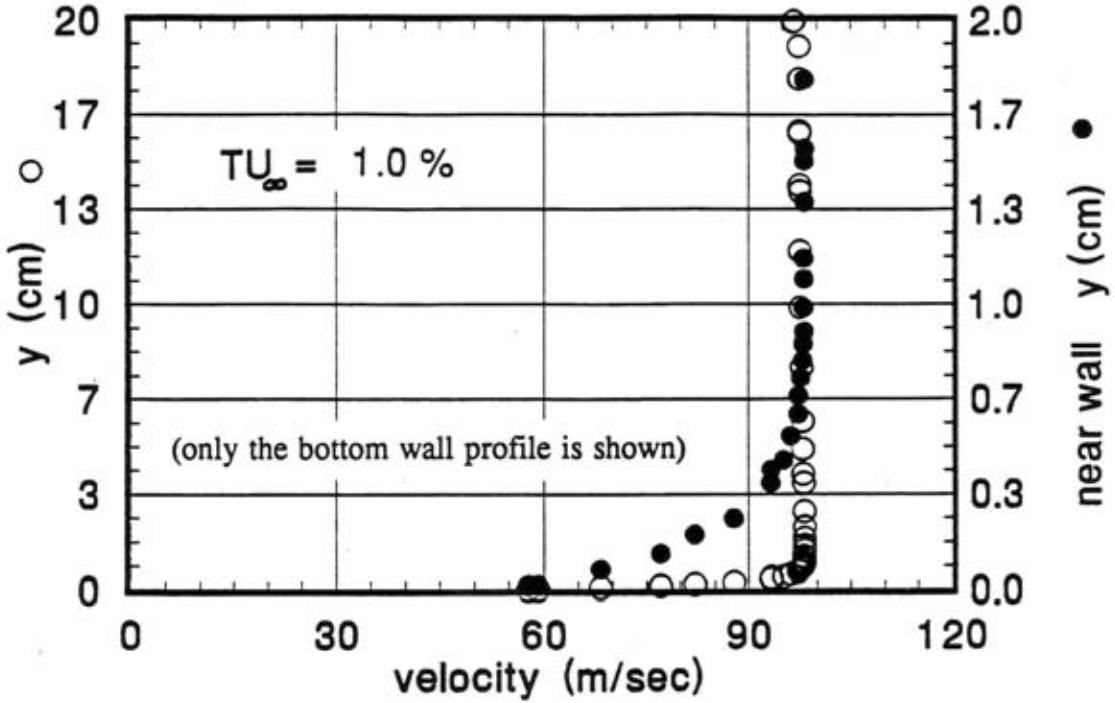

Fig. 4.4 Boundary layer profile at the inlet probe section

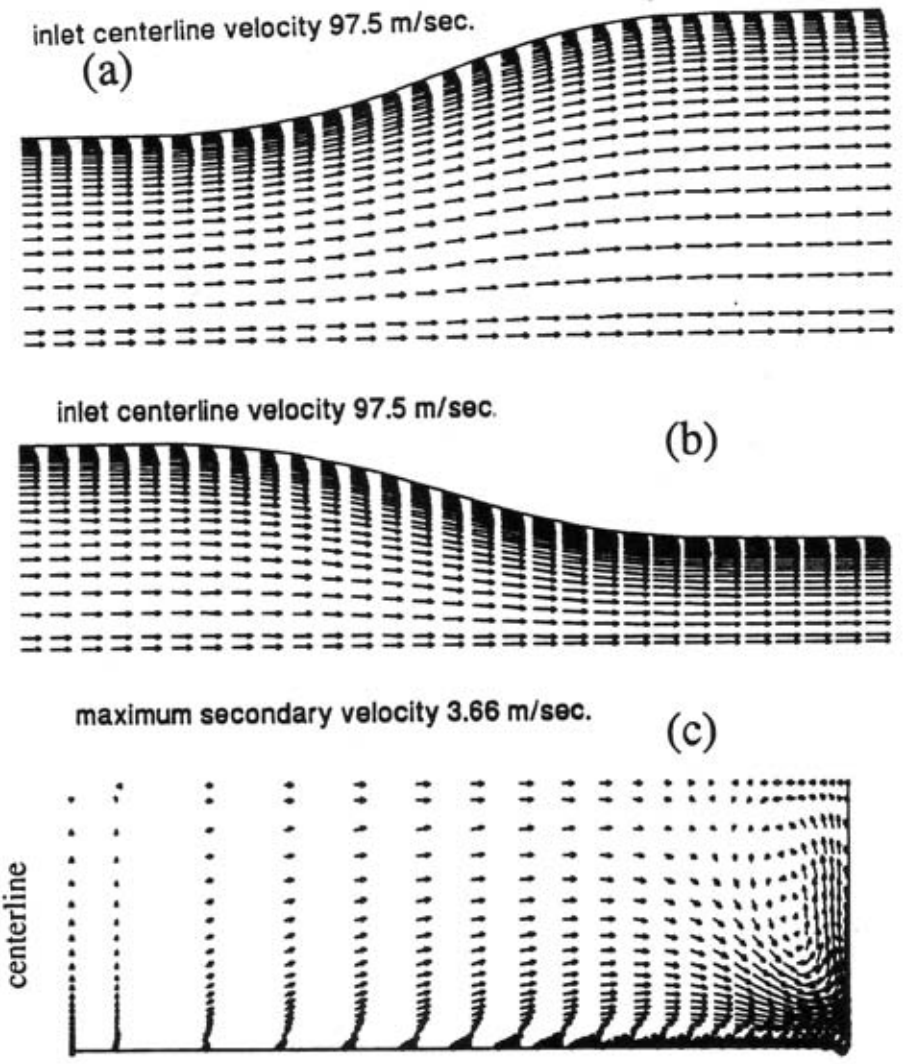

Fig. 4.5 Three dimensional flow predictions in the duct
a. horizontal plane, b. vertical plane, c. secondary velocities

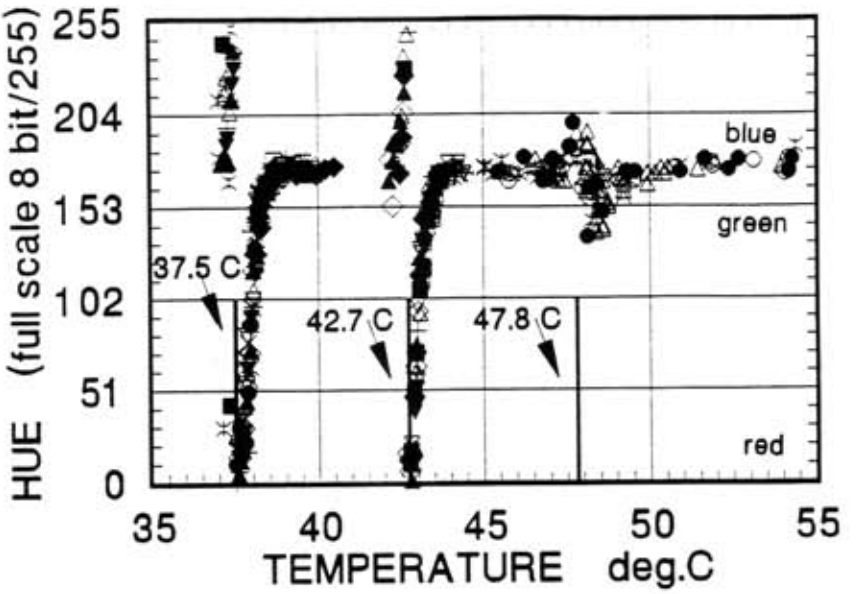

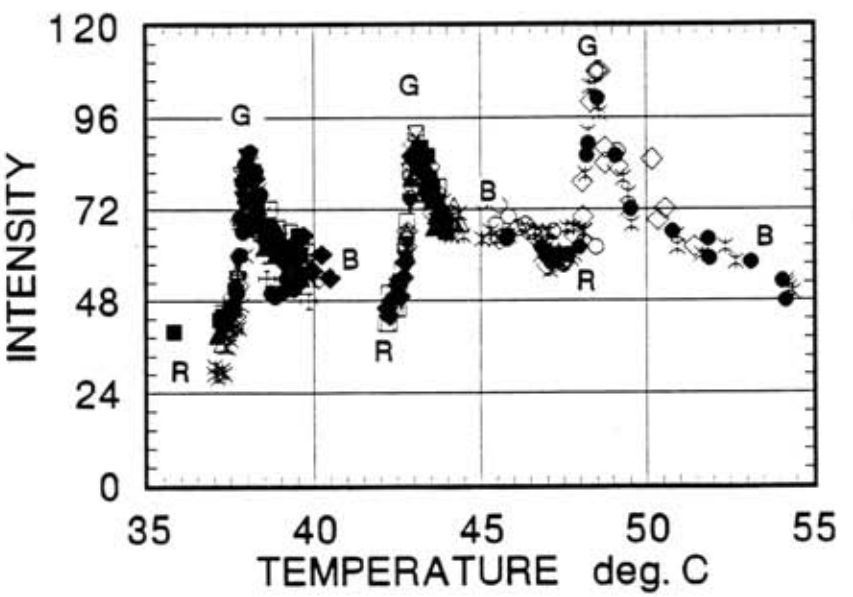

Fig. 4.6 Hue and intensity calibration with respect to temperature

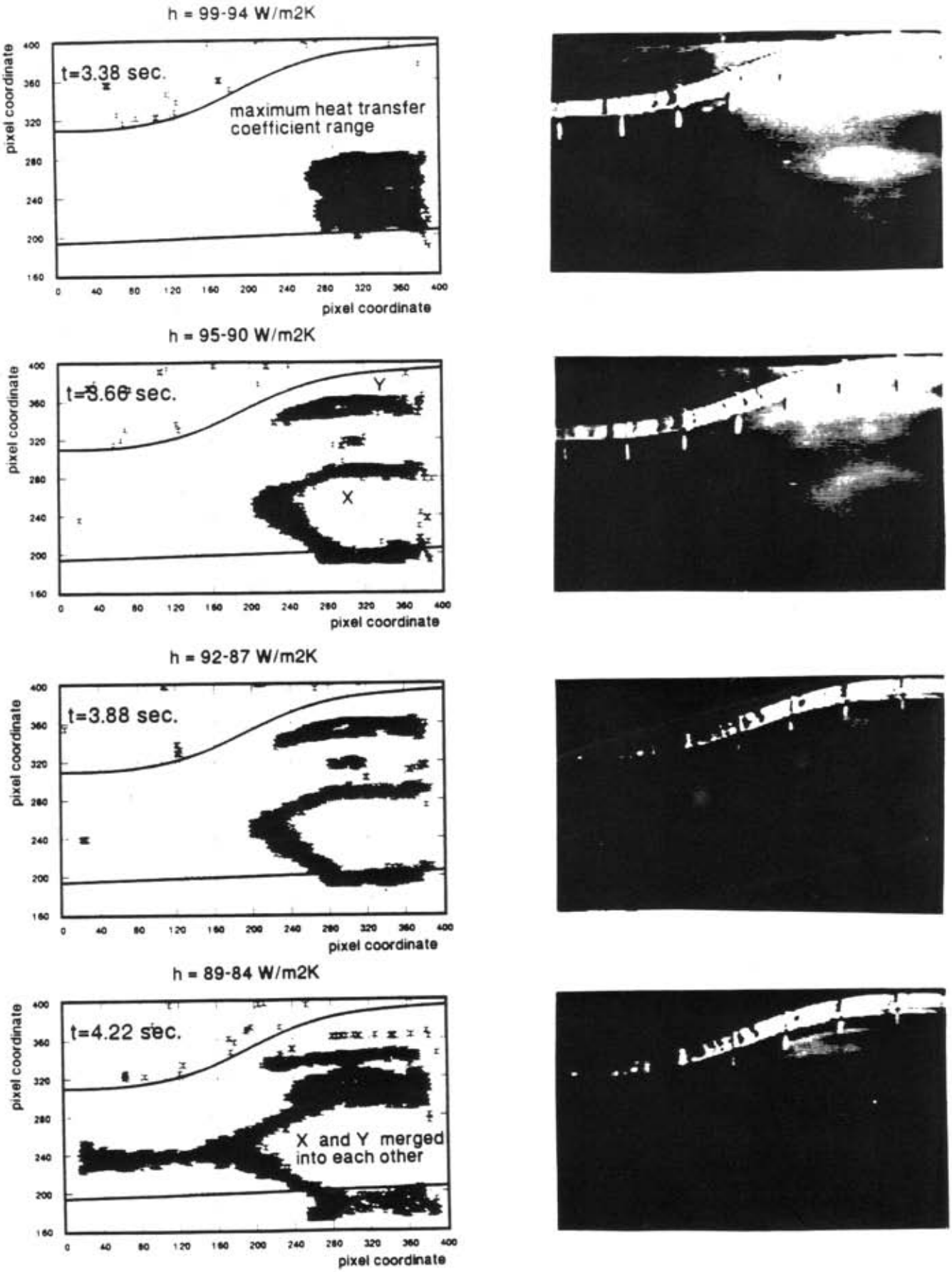

Fig. 4.7.a Convective heat transfer coefficient distributions
t=3.38, 3.66, 3.88, 4.22 sec.

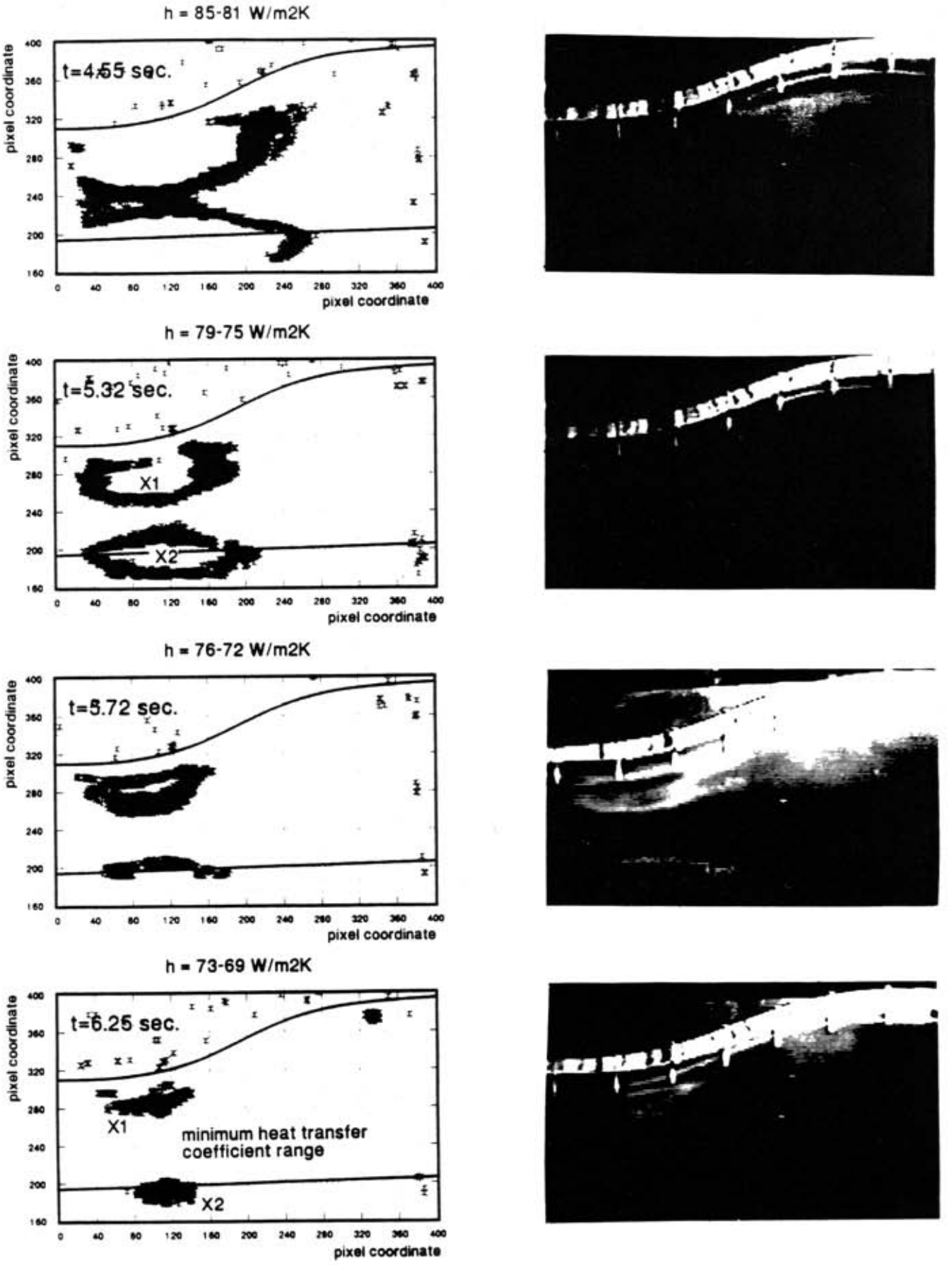

Fig. 4.7.b Convective heat transfer coefficient distributions
t=4.55, 5.32, 5.72, 6.25 sec.

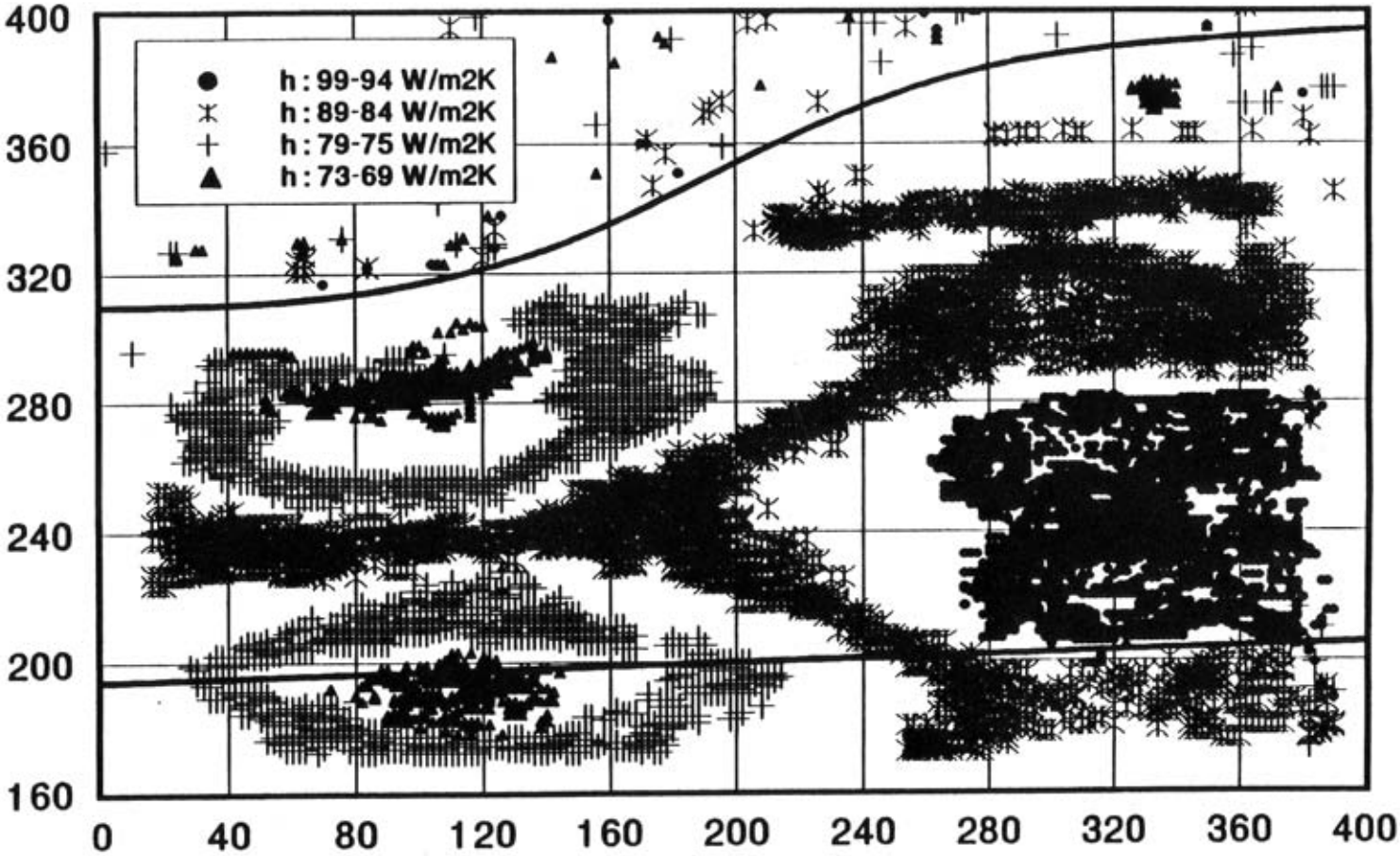

Fig. 4.8 Heat Transfer map at the bottom surface of the transition duct